Materials Today Bio 28 (2024) 101205

Contents lists available at ScienceDirect

Materials Today Bio

journal homepage: www.journals.elsevier.com/materials-today-bio

A self-fused peptide-loaded hydrogel with injectability and tissue-adhesiveness for preventing postoperative peritoneal adhesions

Zequn Zhang [a,c,1], Chao Yin [b,d,1], Xianwen Song [b], Xi Liu [a], Chonglei Zhong [a], Jun Zheng [b], Yaqiong Ni [b], Rujuan Shen [f], Yihang Guo [a], Xiaorong Li [a], Changwei Lin [a], Yi Zhang [b,e,*], Gui Hu [a,**]

[a] Department of Gastrointestinal Surgery, The Third Xiangya Hospital of Central South University, Changsha, 410013, China
[b] Hunan Provincial Key Laboratory of Micro & Nano Materials Interface Science, College of Chemistry and Chemical Engineering, Central South University, Changsha, 410083, China
[c] Department of General Surgery, The Second Xiangya Hospital of Central South University, Changsha, 410011, China
[d] College of Pharmacy, Xinjiang Medical University, Urumqi, 830011, China
[e] National Engineering Research Center for Advanced Polymer Processing Technology, Zhengzhou University, Zhengzhou, 450002, China
[f] State Key Laboratory of Powder Metallurgy, Central South University, Changsha, 410083, China

ARTICLE INFO

Keywords:
Hydrogel
Endostatin
Dynamic crosslinking
Postoperative adhesion
Recurrent adhesions

ABSTRACT

Peritoneal adhesions commonly occur following abdominal or pelvic surgery and can cause serious complications. Currently, physical barriers are the primary approach used in clinical practice to prevent adhesion, although their effectiveness is frequently inadequate. In this study, we developed an injectable peptide-loaded hydrogel with multiple functions, including self-fusion, tissue-adhesiveness, anti-inflammation, anti-cell adhesion and anti-angiogenesis. To assess the effectiveness of these hydrogels, which are stabilized by dynamic imine bonds and acetal connections, in preventing postoperative abdominal adhesions, we utilized both a rat abdominal adhesion model and a rat model simulating repeated-injury adhesions. In comparison to the commercially available HA hydrogel, as-prepared hydrogels exhibited significant reductions in inflammation, fibrosis, and angiogenesis, leading to an obvious decrease in peritoneal adhesions. Moreover, this peptide-loaded hydrogel demonstrated an ideal degradation time, maintaining an in vivo viability for about 10 days. We believe this peptide-loaded hydrogel presents a promising solution for the challenging clinical issue of postoperative abdominal adhesions.

1. Introduction

Post-surgical peritoneal adhesions (PPA) represent a common issue post-operation, potentially leading to complications like obstructive adhesion of the intestines, abdominal discomfort, and possibly infertility [1–3]. In extreme instances, such adhesions may even present a risk to life [4,5]. Although minimally invasive surgery can greatly reduce the formation of adhesions, complete elimination still remains elusive [6]. In clinical practice, pharmacological treatments and physical barriers are commonly employed to counteract intra-abdominal adhesions, while the efficacy of anti-adhesion drugs is often hindered by their limited bioavailability, resulting in suboptimal effectiveness [7–9]. Physical barriers encompass films, polymer solutions, and hydrogels, demonstrating superior anti-adhesion effects compare to drug therapies. Nevertheless, film-type physical barriers necessitate careful attention to hemostasis during application and may not adequately cover irregular wounds [10–12]. Polymer solutions, on the other hand, possess high fluidity but have a short in vivo retention time [13]. Ordinary hydrogels, while excelling at wound coverage, lack specific therapeutic properties. In brief, the crux of the challenge lies in developing an anti-adhesion strategy that harmonizes treatment efficacy, user-friendliness, on-demand degradation, and moldability.

* Corresponding author. Hunan Provincial Key Laboratory of Micro & Nano Materials Interface Science, College of Chemistry and Chemical Engineering, Central South University, Changsha, 410083, China.
** Corresponding author. Department of Gastrointestinal Surgery, The Third Xiangya Hospital of Central South University, Changsha, 410013, China.
E-mail addresses: yzhangcsu@csu.edu.cn (Y. Zhang), hugui22@csu.edu.cn (G. Hu).
[1] These authors contributed equally to this work and should be viewed as co-first authors.

https://doi.org/10.1016/j.mtbio.2024.101205
Received 23 April 2024; Received in revised form 5 August 2024; Accepted 13 August 2024
Available online 14 August 2024

Achieving this delicate balance is crucial in the clinical realm, where the prevention of intra-abdominal adhesions still remains a significant concern in postoperative care. Following abdominal surgery, damage to the peritoneum can trigger a cascade of inflammation and coagulation [14–16]. Excessive coagulation and inflammatory responses sometimes stimulate activated fibroblasts, resulting in the secretion of excessive collagen protein [17,18]. Persistent fibrin bridges can lead to permanent adhesion bands if not dissolved promptly. To enhance the preventive and therapeutic effects of physical barriers in mitigating postoperative adhesions, researchers have explored the incorporation of anti-inflammatory or antioxidant drugs into soft materials. For example, Zeng et al. prepared quercetin-loaded injectable hydrogels via boronate ester bonds, showing promise in preventing postoperative intra-abdominal adhesions [19]. Liu and colleagues developed cream hydrogels based on microgels, incorporating epigallocatechin-3-gallate. These hydrogels demonstrated noteworthy decreases in oxidative stress, inflammation, and fibrosis, and effectively mitigated the development of abdominal adhesions in comparison to the Seprafilm commercial group [20]. Despite these remarkable advancements, there are still many gaps in research on the use of peptides, especially endostatin (ES) with its anti-fibrotic and anti-angiogenic properties, for the prevention of abdominal adhesions. The potential of ES in this regard remains largely unexplored. Currently, ES's effectiveness in inhibiting cancer progression through anti-angiogenic mechanism has garnered widespread recognition. Additionally, the anti-fibrotic efficacy of ES has been substantiated across diverse fibrosis models, laying a solid theoretical groundwork for its potential use in abdominal adhesion management. Using hydrogels as carriers for ES could address stability and availability challenges, offering a promising solution for effective treatment. Such endeavors should take into account the equilibrium between treatment efficacy and simplicity of application in clinical environments.

This paper introduces a challenging attempt to integrate both physical barrier and pharmacotherapy strategy to prevent post-surgical peritoneal adhesions by building up a stable drug load hydrogel dress with anti-inflammatory, anti-angiogenesis, and anti-fibrosis abilities. Inspired by those pioneering advances, and as a continual work of our previous studies [21,22], we here selected two raw materials, carboxymethyl chitosan (CMCS) and poloxamer F127 (F127). CMCS has been widely used in many clinical situations, such as promoting wound healing, hemostasis, analgesic and bacteriostatic effects [23,24], owing to its unique biocompatibility, biodegradability, antimicrobial activity, low immunogenicity, mucoadhesion [25,26]. F127 is an important biomaterial with good affinity for peptide drug molecules [27], commonly used for delivering therapeutic proteins and peptides to combat various incurable diseases [28–30]. However, the mechanical properties of hydrogels prepared directly by mixing CMCS with F127 are insufficient to meet the requirements for prevention and treatment of postoperative abdominal adhesion. Therefore, in order to achieve better mechanical strength, this study chose glyoxal as a crosslinking agent to enhance the mechanical properties of the hydrogels. Glyoxal, the smallest dialdehyde and an endogenous aldehyde, can adjust the mechanical properties of the hydrogel by forming schiff base bonds between its aldehyde groups and the amino groups of carboxymethyl chitosan, as well as acetal bonds with the hydroxyl groups of carboxymethyl chitosan and F127 [31]. While glyoxal has been associated with contact dermatitis [32], studies have shown that only free glyoxal possesses toxicity [33], whereas cross-linked glyoxal after reacting with raw materials is non-toxic. Compared to most chemical crosslinking agents, it exhibits lower cytotoxicity and has been utilized in research fields such as bone tissue repair, tissue regeneration, and surgical sutures [34–36]. To confer additional therapeutic benefits, ES with anti-angiogenic and anti-fibrotic properties was incorporated into the hydrogel matrix. This ES-loaded hydrogel not only overcomes the potential hazards of high-dose short-term intravenous or intraperitoneal administration, and the drawback of rapid peritoneal clearance, but also addresses the limitation of simple physical barriers that fail to effectively function in the pathogenesis of adhesion development. A comprehensive evaluation of the PXCE hydrogel was undertaken, encompassing injectability, self-healing capacity, moldability, rheological characteristics, in vitro ES release profile, anti-inflammatory potential, anti-angiogenic effects, anti-fibrotic activity, tissue adhesiveness, hemolysis, and biocompatibility. Subsequently, we established a rat model for abdominal adhesions and a rat model involving repeated injury after adhesiolysis to evaluate the effectiveness of the PXCE hydrogel in preventing postoperative abdominal adhesions. Our experiments results highlight the significant potential of PXCE hydrogel, which possess the ability to release ES while exhibiting adhesive properties and moldability, demonstrating the efficacy of PXCE hydrogel in promoting the prevention of postoperative abdominal adhesions.

2. Experimental section

2.1. Materials

Endostatin (ES) (5 mg/mL, Mw: ~20 kDa) was purchased from Shandong Simcere Bio-Pharmaceutical Co., Ltd., Carboxymethyl chitosan (CMCS) with an 80 % substitution degree was purchased from Yuanye, Poloxamer F127 (F127), methylene blue, and methyl orange were obtained from Aladdin. Glyoxal solution (Gly, 40 wt%) was obtained from Macklin, PBS (pH 7.4) was obtained from Churui Bio-Technology Co., Ltd.

2.2. Preparation of injected CMCS/F127/ES hydrogel

F127 and CMCS were dissolved separately in deionized water to create a uniform solution with varying mass ratios of 1:1, 2:1, and 3:1. Subsequently, 0.75 mL of Glyoxal solution (1 wt%) was introduced into each solution and stirred for 1 h. Next, the hydrogels were dialyzed exhaustively against water. They were named PXC1, PXC, PXC3, respectively. For the ES-loaded PXC, the PXC was soaked in an ES solution for 2 days at 4 °C, and the prepared hydrogel was named PXCE.

2.3. Characterizations

Scanning Electron Microscopy (SEM, JEOL JEM-2010, Japan) was utilized for observing the morphology of lyophilized PXC1 hydrogel, PXC hydrogel, PXC3 hydrogel, and PXCE hydrogel. Fourier Transform Infrared Spectroscopy (FT-IR, Nicolet iS50, Thermo, USA) was applied to confirm the chemical structure of CMCS, F127, PXC hydrogel, and PXCE hydrogel. The crystalline behavior of CMCS, F127, PXC hydrogel, and PXCE hydrogel was investigated by X-ray diffraction.

2.4. The rheological studies

The rheological properties of the hydrogels were assessed by a rheometer (Discovery HR-1, TA, USA). The storage modulus (G′) and loss modulus (G″) of PXC1, PXC, PXC3, and PXCE hydrogel were determined via frequency-sweep mode within the frequency range of 0.1–100 rad s^{-1}, maintaining a fixed strain of 1 % at 25 °C. An oscillation strain sweep of four hydrogels was conducted over a strain range of 0.1%–10000 % at 6.28 rad s^{-1}. The viscosity of PXCE hydrogel was measured across a shear rate range of 0.1–100 s^{-1}. To validate the capacity of PXCE hydrogel to recover from strain deformation, step-strain-sweep tests were performed, alternating between an oscillation strain of 1 % and 800 % for a total of five cycles.

2.5. Self-healing behavior of the hydrogel

The PXC hydrogel and PXCE hydrogel were stained with methylene blue and methyl orange, respectively, to evaluate the self-healing properties of the two hydrogels. Both the unstained block hydrogels and the stained hydrogels were sliced into two halves, placed side by

side under room temperature conditions for observation.

2.6. Swelling properties

The hydrogels, after being dried and weighed, were immersed in 5 mL of PBS (0.01 M, pH 7.4) at 37 °C. Their weights were measured at specific intervals. The swelling ratio (SR%) of the hydrogels was calculated using the following formula:

$$SR\% = (W - W_0) / W_0 \times 100$$

Here, W and W_0 represented the weights of hydrogels at distinct time points and the initial weight of the dry hydrogels, respectively. Each sample was tested three times.

2.7. ES release of PXCE hydrogel

The release profile of ES from the PXCE hydrogel was examined by a shaking water bath (37 ± 0.5 °C, 80 rpm). 1 mL PXCE hydrogel containing 2 mg of ES was placed in PBS solution and incubated in the shaking water bath. At specific time intervals, 0.3 mL sample was withdrawn, and 0.3 mL fresh PBS solution was added back to the release medium. The amount of ES released at various time points was quantified using ELISA.

2.8. Cytotoxicity evaluation and antifouling properties of PXCE hydrogel

The cytotoxicity of PXCE hydrogel on human peritoneal mesothelial cell line, HMrSV5, was thoroughly evaluated utilizing the CCK-8 assay. The HMrSV5 cell line, obtained from the esteemed cell bank of the Chinese Academy of Medical Sciences in Beijing, was cultured in 1640 medium supplemented with 10 % FBS (fetal bovine serum, Gibco), and anintained in an environment of 5 % CO_2 at 37 °C. The cytotoxicity of PXCE hydrogel at different concentrations (25–1600 μg mL^{-1}) was detected. In addition, the cytotoxicity of CMCS solution, F127 solution and PXC solution, each at a concentration of 1600 μg mL^{-1}, as well as the ES solution (30 μg mL^{-1} ES in 1600 μg mL^{-1} PXCE solution), were individually assessed. The experimental protocol was as follows: HMrSV5 cells were seeded into a 96-well plate at a density of 5000/well (n = 6). Following a 24-h incubation period, the hydrogel samples were added and further incubated for 24–72 h. At predetermined time points, 200 μL medium containing 10 μL of CCK-8 (GeneView) was added to each well, and the absorbance at 450 nm was measured with a microplate spectrophotometer (Thermo Fisher) after incubation at 37 °C for 2 h. The experimental data were standardized with the control group without any intervention, and the results were expressed as mean ± SD.

Cell-adhesion assays were conducted to assess the antifouling properties of PXC and PXCE hydrogels. To investigate fibroblast attachment onto the surface of equilibrated hydrogels, discs of PXC and PXCE hydrogels were placed in triplicate in 48-well plates. Mouse fibroblasts (L929, purchased from the Shanghai Chinese Academy of Sciences Cell Bank) in the logarithmic growth phase were then seeded into each well at a density of 1×10^4 per well. Following a 48-h incubation period, the supernatants were discarded, washed by PBS and loosely adherent cells. Subsequently, the cell adhesion on the surface of hydrogel samples was observed and photographed using a microscope (Carl Zeiss, Germany). The cells without any hydrogel samples were used as the control group.

2.9. Experimental animals

Male adult Sprague-Dawley (SD) rats (220 ± 20 g) were purchased from the Department of Laboratory Zoology, Central South University. All animal experimental procedures were carried out by the Guide for the Care and Use of Laboratory Animals (National Research Council, USA). This study was approved by the Institutional Animal Care and Use Committee of Central South University (2020sydw0971).

2.10. Establishment of the rat abdominal adhesion model

The sidewall-cecum abrasion model was established. Twenty-four male rats were categorized into four experimental groups: control group, HA hydrogel (Commercial anti-adhesion product, also known as Hairont, produced by Zhejiang Jingjia Medical Technology Co., Ltd.), PXC hydrogel and PXCE hydrogel. Initially, wounds of approximately 3 × 1.5 cm^2 were created on the abdominal wall and cecum of the rats. Subsequently, 1 mL of the respective hydrogel was injected onto the wounds of the HA, PXC, and PXCE groups, while the wounds of the control group received no treatment. Euthanasia of the rats was performed at one- and two-weeks post-surgery, and the degree of wound adhesion was assessed and scored (0–5), with higher scores indicating more severe adhesion [37,38].

2.11. Establishment of rat repeated-injury adhesion model after adhesiolysis

To evaluate the hydrogel's capacity in preventing recurrent adhesion, the repeated-injury adhesion model were established [39,40]. Initially, the rat cecum-abdominal wall adhesion model was established without treatment with anti-adhesion materials. One week later, adhesiolysis was conducted to induce repeated injury. Following the reopening of the incision, the adhesion site resulting from the initial operation was meticulously separated using blunt or sharp dissection as required. Subsequently, 1 mL of PXC, PXCE, or HA hydrogel was applied to the re-injured site. The untreated control group replicated the conditions of the initial model. On day 7 following the second surgery, the rats were euthanized. The subsequent steps accorded with the first model.

2.12. Histology and immunohistochemistry

Various tissues (adhesion tissues and major organs) were gathered for histological assessment of toxicity. Following fixation, embedding, and subsequent sectioning, the tissues were subjected to staining with hematoxylin and eosin (H&E), Masson trichrome, and immunohistochemistry antibodies. Imaging of the slides was carried out utilizing a microscope (Carl Zeiss, Germany).

After fixation, embedding, and sectioning of the specimens, antigen retrieval was placed in a repair box using citric acid antigen retrieval buffer (pH 6.0). The primary antibodies employed were as follows: α-SMA (1:2000, GB111364, Servicebio), CD31 (1:500, GB113151, Servicebio). Subsequently, the sections were stained with DAB substrate chromogen solution and counterstained with hematoxylin. Two blinded investigators quantified positively stained cells or areas within five normalized high-power fields utilizing both an Axiostar Plus microscope by Carl Zeiss, Germany and ImageJ software developed by NIH.

2.13. ELISA analysis of blood sample

On the 7th day after the initial surgery, blood samples were obtained from rats, then left at room temperature for 1 h before centrifugation to collect serum. The abundance of IL-6, TNF-α, and TGF-β1 were detected by ELISA kits (Proteintech).

2.14. Hemolysis assay

After isolation by centrifugation and washing with PBS buffer, the red blood cells (RBCs) were diluted to 5 % (v/v). Subsequently, the PXCE hydrogel (100 μL or 500 μL) and the RBCs suspension (500 μL) were added to a 1.5 mL centrifuge tube, respectively. The tube was then topped up with PBS and incubated at 37 °C in a shaking incubator at 100 rpm for 1 h, following incubation, the contents of the tube were centrifuged, the supernatant was collected, and the absorbance was measured at 540 nm using a microplate reader. A positive control

utilizing Triton X-100 (0.1 %) and a negative control with PBS buffer were established. The hemolysis rate was calculated using the following equation:

$$Hemolysis\ rate\% = (A_p - A_b) / (A_t - A_b) \times 100\%$$

Where A_p, A_t and A_b represent the absorbance of the test group, positive control, and negative control, respectively.

2.15. In vivo retention study

FITC-labeled PXC and PXCE hydrogels were applied to a rat model of sidewall defect-cecum abrasion [41]. The aforementioned abdominal adhesion model was constructed, and 1 mL of FITC-labeled PXC or PXCE hydrogel was injected to cover the injured surface. Three rats per group were taken at each time point at 0 (2h), 3, 7, 10, and 14 days after the operation. Specifically, laparotomy was performed, and the fluorescence intensity was collected under a small animal in vivo imager (IVScope capture, CLiNX Science Instrument).

2.16. Statistical analysis

The statistical analysis utilized SPSS 25.0 (Chicago, IL, USA). The results were represented as means ± SD. GraphPad Prism 8 was employed for conducting one-way ANOVA analysis to assess the significance of differences among three or more groups, with a significance level set at $p \leq 0.05$.

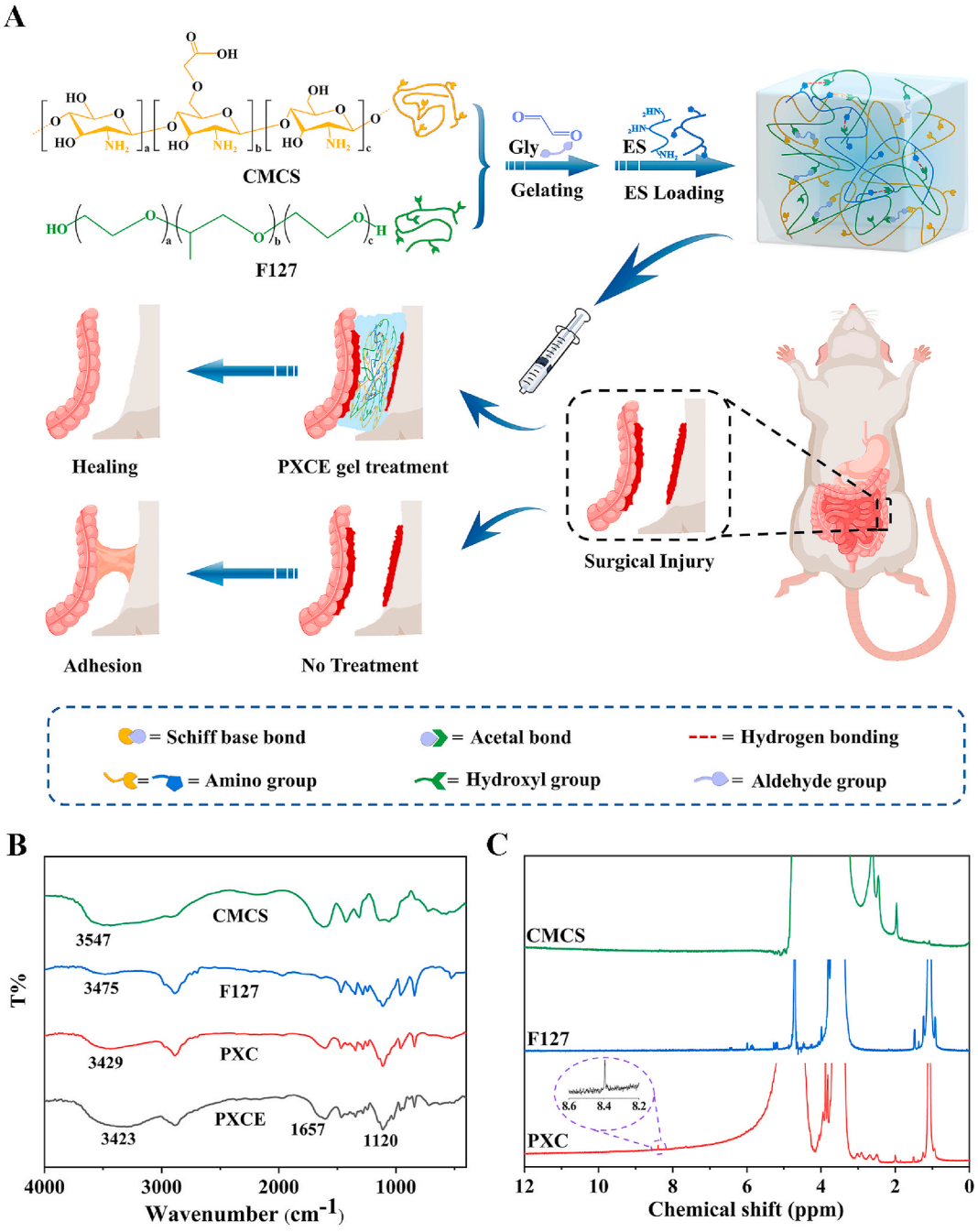

Fig. 1. Preparation of self-fused and injectable peptide-loaded hydrogel. A) Schematic diagram of the self-fused and injectable peptide-loaded hydrogel formation and the prevention of postoperative peritoneal adhesions; B) FT-IR spectra and C) ^{1}H NMR spectra of CMCS, F127, PXC hydrogel, and PXCE hydrogel.

3. Results and discussion

3.1. Fabrication and characterization of hydrogels

The self-fused and tissue-adhesive peptide-loaded hydrogel with suitable mechanical properties and good biocompatibility was formulated by utilizing the double dynamic bond of imine bonds and acetal linkages. Fig. 1A illustrated the overall strategy of developing the PXCE hydrogel for preventing post-surgical peritoneal adhesions. To optimize the mechanical properties of hydrogels, we prepared three types of PXC hydrogels with final mass concentration ratios of CMCS to F127 at 1:1 (PXC1), 1:2 (PXC), and 1:3 (PXC3), respectively, and investigated the influence of polymer concentration on the gelation time of the hydrogels. As depicted in Fig. S1, a significant decrease in gelation time was observed with an increase in the final mass concentration ratio of CMCS to F127. Specifically, when the mass concentration ratio of CMCS to F127 was 1:3, the average gelation time was 60 ± 7 s. As the ratio decreased from 1:3 to 1:2, the gelation time increased to 300 ± 18 s, whereas the PXC hydrogel with a 1:1 ratio of CMCS to F127 failed to form a stable gel. This can be attributed to the fact that higher concentrations of CMCS and F127 may enhance the probability of reactions between aldehyde groups with amino and hydroxyl groups. Based on the PXC group, we further added ES to prepare PXCE, and Fig. 2S indicates that the addition of ES did not significantly impact the steady-state structure of the PXC hydrogels.

The FT-IR findings suggest that, compared to PXC hydrogel, the O–H and C=O stretching vibrations were shifted to lower wavenumbers, indicating the formation of hydrogen bonds and electrostatic interactions upon the addition of ES [42,43]. Additionally, the FT-IR analysis demonstrates the appearance of two new infrared bands at 1657 cm^{-1} and 1120 cm^{-1}, corresponding to the C=N and C–O–C stretch, respectively [44,45] (Fig. 1B). The schiff base bond of the PXCE

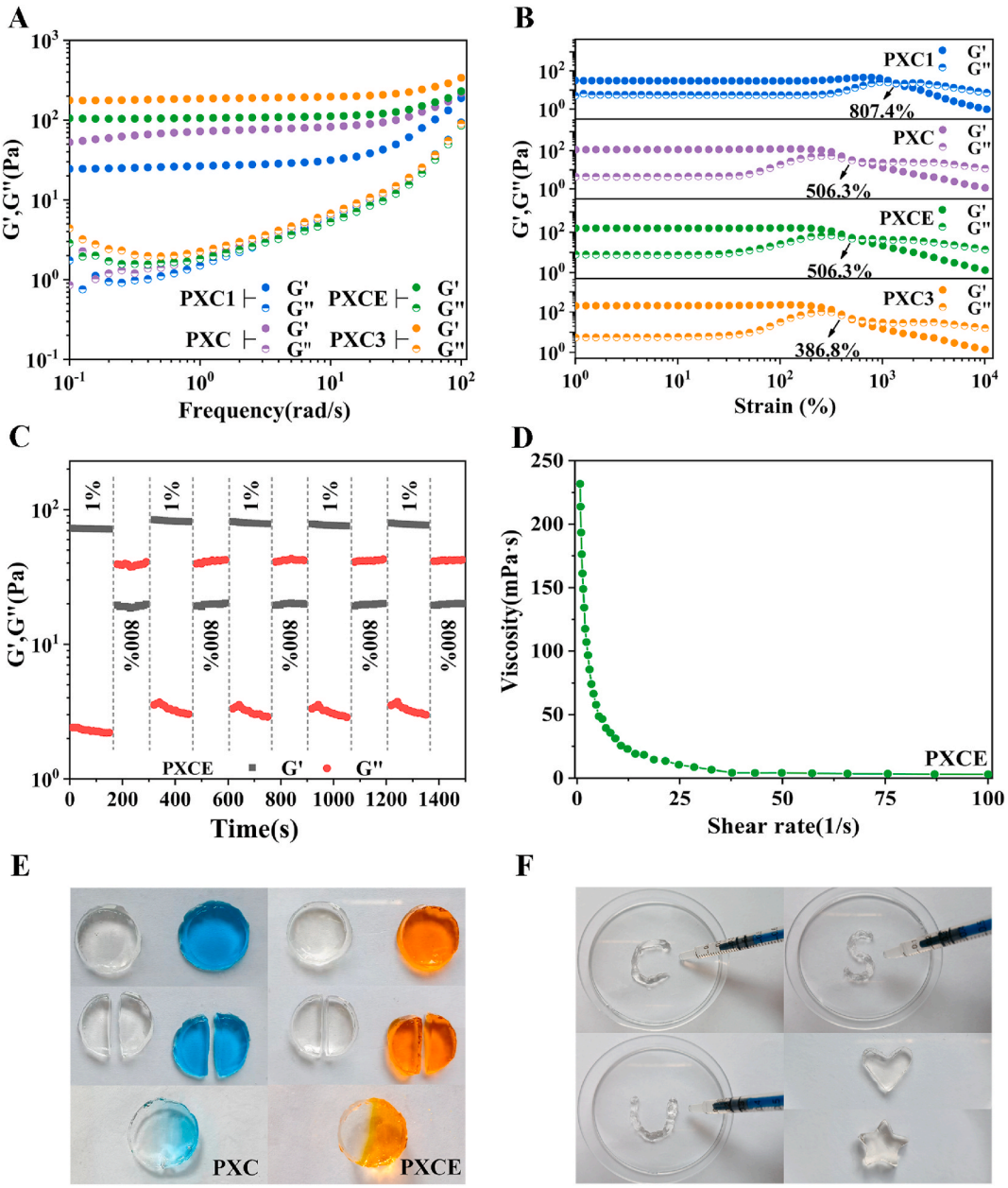

Fig. 2. Self-healing and injection ability of the hydrogel. A) Frequency-dependent curves of PXC and PXCE; B) Strain-dependent curves of PXC and PXCE; C) Step strain sweep curves of PXC and PXCE; D) Shear rate sweep of PXC and PXCE; E) Macroscopic self-healing process of PXC and PXCE; F) Photographs of the injectability and moldability of PXCE.

hydrogel is further confirmed via ^{1}H NMR spectroscopy, which indicates distinct peaks of imine protons at 8.4 ppm, absent in CMCS and F127 (Fig. 1C).

Zeta potential, a physicochemical property, is utilized to evaluate the interactions between charged polypeptides and polysaccharides [46]. As depicted in Fig. 3S, the zeta potential of ES measures at 6.96 ± 2.58 mV. zeta potential of PXC hydrogel is −10.90 ± 3.67 mV, which may be attributed to the carboxyl groups of CMCS, and the electronegative oxygen atoms of PEO segments in F127 [47,48]. After loading ES, the zeta potential of PXCE hydrogel shifts to −4.71 ± 1.09 mV. Due to the electrostatic interactions between ES and the PXC hydrogel, the absolute value of the zeta potential of PXCE is lower than that of the PXC hydrogel. The results of zeta analyses are consistent with the observations from FT-IR.

The structural details of as-prepared hydrogels were assessed using SEM, revealing non-uniform and interconnected porous microstructures for all hydrogel, indicating that the adequate loading of endostatin ES without causing unnecessary alterations to the network structure (Fig. S4A–D). Fig. S4E–H shows that the pore size of the hydrogel gradually decreases with the increase of F127 mass concentration in the hydrogel. This phenomenon may be caused by the increase of F127 mass concentration, the increase of molecular entanglement, and the increase of cross-linking density, so the pore size of the hydrogel decreases. Specifically, the average pore size of the PXC hydrogel is 12.34 μm, whereas that of the PXCE hydrogel is 9.53 μm, smaller than that of the PXC hydrogel. This is likely due to the amino and carboxyl groups in ES that can form hydrogen bonds and electrostatic interactions with the PXC hydrogel, leading to a higher crosslinking density and consequently smaller pore sizes [49–51]. The molecular weight of ES is about 20 kDa and the size is about 1.8 nm, which is much smaller than the pore size of PXC hydrogel (12.34 μm), indicating that ES can be adsorbed not only on the surface, but also in the hydrogel matrix.

In order to investigate alterations in the crystalline structure, XRD tests were performed. The XRD spectra, as depicted in Fig. S5, demonstrated that CMCS existed in an amorphous phase, exhibiting a weak peak at 20.1° [52]. In contrast, the F127 spectra exhibited two distinct sharp peaks at 19.2° and 23.4°, these peaks had been reported previously [53]. Notably, in comparison to F127, the intensity of characteristic peaks of F127 in the PXC hydrogel was insignificant, indicating that the formation of the PXC hydrogel inhibited the crystalline nature of F127. Upon the addition of ES into the PXC hydrogel, new peaks were observed at 9.8°, 20.6°, 21.3°, and 22.1°, illustrating the presence of ES in the PXCE hydrogel.

3.2. Rheological properties, swelling ratio, and drug release properties of hydrogels

Rheological tests were performed to assess the viscoelastic properties of the prepared hydrogels. During the frequency sweep test (Fig. 2A), it was noted that the G′ predominated over the G″ across the frequency range from 1 to 100 rad s^{-1}, indicating the hydrogel's typical elastic behavior under all testing conditions. As the F127 ratio increased from PXC1 to PXC3, there was a simultaneous increase in the values of G'. This phenomenon can be attributed to the entanglement of F127, which leads an augmentation of cross-linking density within the hydrogel matrix. Moreover, the values of both G′ and G″ for the hydrogels exhibited an increase at higher frequencies, which can be attributed to the establishment of dynamic networks within the hydrogel structure [54]. Compared to the PXC hydrogel, the PXCE hydrogel consistently exhibited higher G′ values, suggesting the formation of hydrogen bonds between ES and F127. This finding aligned with the results obtained from the frequency-sweep test. The intersection points of the G′ and G″ curves, as depicted in Fig. 2B, exhibited a reduction with increasing mass of F127. Beyond the point where the strain force surpassed the intersection of the G′ and G″ curves, the 3D network of the hydrogel was disrupted. In general, a higher storage modulus indicates greater rigidity, which is unfavorable for injection purposes. Considering these factors both the PXC hydrogel and PXCE hydrogel were chosen as the

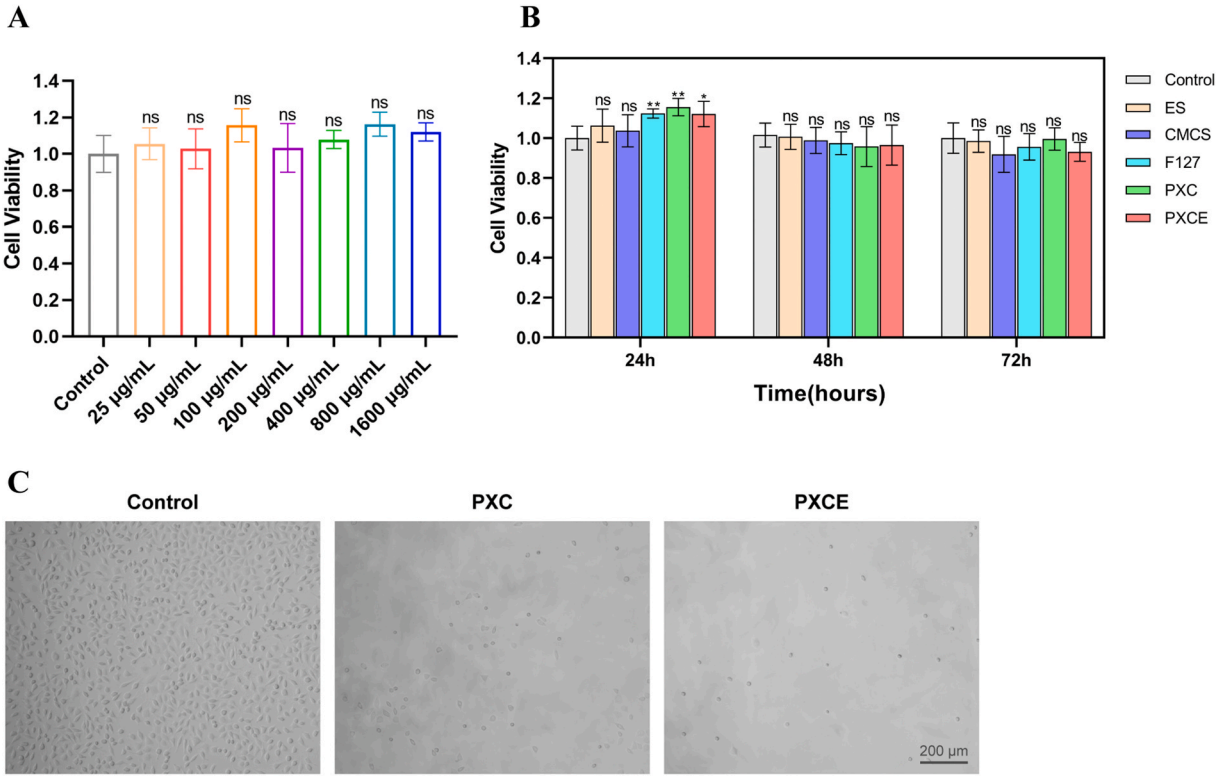

Fig. 3. Cell viability and the resistance for fibroblast adhesion of PXCE hydrogel. A) Cytotoxicity of PXCE hydrogel in different concentrations; B) Cytotoxicity of different components of PXCE hydrogel; C) Cellular attachment of HMrSV5 on control, PXC hydrogel, and PXCE hydrogel (n = 5).

barrier for preventing abdominal adhesion in follow-up experiments.

The swelling behavior of the hydrogels were investigated at 37 °C. It was observed that with an increase in the mass of F127, the swelling ratios exhibited a decrease (Fig. S6A). This outcome can be attributed to the greater mass of F127, which promotes a more compact network structure within the hydrogel. The addition of ES possibly enhanced the cross-link density of the PXCE hydrogel, resulting in a reduced swelling rate and water absorption compared to the PXC hydrogel. This property is advantageous in averting postoperative abdominal adhesion.

The study also examined the sustained release behavior of ES within the PXCE hydrogel using ELISA. Fig. S6B showed that the PXCE hydrogel exhibited sustained release of ES for 168 h, and the release process was divided into two stages. During the first 96 h, ES in the PXCE hydrogel exhibited a quick release process, with a cumulative release ratio of 14.09 %. This rapid release observed initially may be attributed to the ES adsorbed on the surface of the PXCE hydrogel and physical diffusion. Subsequently, after 96 h, the release curve changed into a slow and steady process, resulting in a total release rate of 14.93 % after the sustained release period of 168 h. These results suggested that the PXCE hydrogel prolonged the release duration of ES, thus enhancing its efficacy and showcasing promise in mitigating post-operative peritoneal adhesion.

3.3. Self-healing, injectability, and shape adaptation of hydrogels

The hydrogel's inherent self-healing nature is advantageous in maintaining the structural integrity of its network and functioning as an effective barrier against abdominal adhesion. As depicted in Fig. 2C, the self-healing ability of the PXCE hydrogel were evaluated by continuous amplitude step strain measurements. Under a small strain of 1 %, the G′ of the PXCE hydrogel exceeded the G″, indicative of its gel-like state. As the strain increased from 1 % to 100 %, the G″ of the PXCE hydrogel surpassed G′, causing the destruction of the hydrogel network and its transition into a fluid-like state. Intriguingly, upon the strain returned to 1 %, the initial moduli of the PXCE hydrogel were almost entirely recovered, demonstrating the excellent recovery capability of the PXCE hydrogel. The macroscopic self-healing assay was conducted to further evaluate the self-healing capability of both the PXC hydrogel and PXCE hydrogel. The PXC hydrogel and PXCE hydrogel, loaded with methylene blue and methyl orange, were cut into two parts and spliced together with the corresponding unstained hydrogel, healing for 2 h at room temperature (Fig. 2E). These two semicircles with different colors fused into a complete hydrogel through schiff-base bonds and hydrogen bonds, suggesting the remarkable self-healing ability of both the PXC hydrogel and PXCE hydrogel.

In the realm of minimally invasive surgeries, the injectability of hydrogels holds paramount importance, bearing considerable clinical significance. Shear-dependent viscosity was used to assess the injectability of the as-prepared hydrogels. Our experimental results revealed a decrease in the viscosity of the PXCE hydrogel with increasing shear rates (Fig. 2D), demonstrating that the PXCE hydrogel with good shear-thinning properties is advantageous for injection to prevent abdominal adhesion. Furthermore, the PXCE hydrogel demonstrated further versatility in its injectability, as it could be molded into the shape of "CSU" and other desired forms by injecting it into differently shaped molds, such as hearts and pentagrams (Fig. 2F). This feature highlights the potential of the PXCE hydrogel for precise shape control and customization in various applications.

3.4. Cytotoxicity evaluation of PXCE hydrogel

The cytotoxicity of PXCE and PXC hydrogels was detected by CCK-8 assay, respectively. As illustrated in Fig. 3A, the cell viability of PXCE hydrogel at various concentrations exceeded 98 %, showing no statistical difference compared to the control group. Furthermore, we also assessed the cytotoxicity of different components of PXCE hydrogel as well as PXC hydrogel. Consistent with the above results, the components of PXCE and PXC hydrogels also did not demonstrate significant cytotoxicity (Fig. 3B). Taken together, the PXCE and PXC hydrogels had good cytocompatibility and are safe and reliable, which aligned with the objective of our design. The safety of the hydrogels is critically important and needs to be considered primarily, thus we have deliberately selected components (CMCS and F127) with excellent cytocompatibility to ensure the safety of the synthesized samples.

3.5. Assessment of cell adhesion on the surface of PXCE hydrogel

Peritoneal adhesions are largely formed through fibrosis, which serves as a critical mechanism. In vivo, peritoneal mesothelial cells (PMC) typically undergo a process called mesothelial-mesenchymal transition (MMT), transforming into myofibroblasts. These myofibroblasts secrete collagen, facilitating the formation of adhesions. Fibroblasts, generally prompted by various factors such as inflammation, become activated, proliferate, and begin secreting components of the extracellular matrix (ECM), including collagen. Subsequently, they contributed to the formation of granulation tissue that fills defected and promoted wound healing. In essence, fibroblasts play a key role in triggering tissue overgrowth and initiating adhesion formation. The cell attachment for PXC, PXCE, and the control group was shown in Fig. 3C. The control group displayed a significant presence of proliferating spindle cells and irregular polygonal cells (L929 cell line). Conversely, the PXC group exhibited sparse irregularly shaped fibroblasts and suspended round cells. Interestingly, the PXCE group exhibited the most prominent effects and contained only a small number of circular suspended cells together with individual irregular-shaped cells. The circular suspended cells are cells that are not attached or adhered to the surface of the hydrogel. To summarize, both PXCE and PXC hydrogels exhibited significant inhibitory effects on fibroblast adhesion, and the performance of the PXCE group was even better. This could be partly due to the inhibitory effect of sustained ES, which was consistent with the previous studies suggesting that ES inhibited the proliferation of scar fibroblasts [55,56].

3.6. Evaluation of anti-adhesion efficacy on primary postoperative peritoneal adhesions in sidewall-cecum abrasion model

The in vivo anti-adhesion properties of PXC and PXCE hydrogels were assessed using a rat model of sidewall-cecum abrasion, with HA hydrogel serving as the control. The extent of adhesion was assessed (Fig. 4A) and scored (Fig. 4B, C and 4D) through laparotomy on days seven and 14 after the operation. High average adhesion scores were observed in the control group, indicating severe adhesions. The adhesion bands were compact and could not be bluntly dissected with surgical forceps. In the group treated with HA hydrogel, rats still experienced varying degrees of adhesion. Although the average scores were lower compared to the untreated group, they remained relatively high, indicating unsatisfactory anti-adhesion efficacy of HA hydrogel. The effectiveness of PXC hydrogel was marginally superior to that of HA hydrogel, potentially attributable to the antibacterial and anti-inflammatory properties of CMCS components. In contrast, the HA hydrogel barely induced a single physical barrier effect. Among the treatment groups, PXCE hydrogel exhibited the lowest score, with almost no observed adhesion. By day 7, the injured surfaces of the cecum and abdominal wall had largely returned to normal, with only slight peritoneal scars evident and a thin layer of collagen deposition in the subperitoneum. By day 14, the injured surface was smooth and flat, and completely returned to normal state. The improved anti-adhesion efficacy of PXCE compared to PXC can be attributed to the inclusion of ES into PXCE, which had anti-angiogenesis and anti-fibrosis functions. The incorporation of ES into the hydrogel allows for a controlled, sustained release of the substance at a lower dosage, further enhancing its efficacy in preventing tissue adhesion. Fig. 4E depicted the distribution of

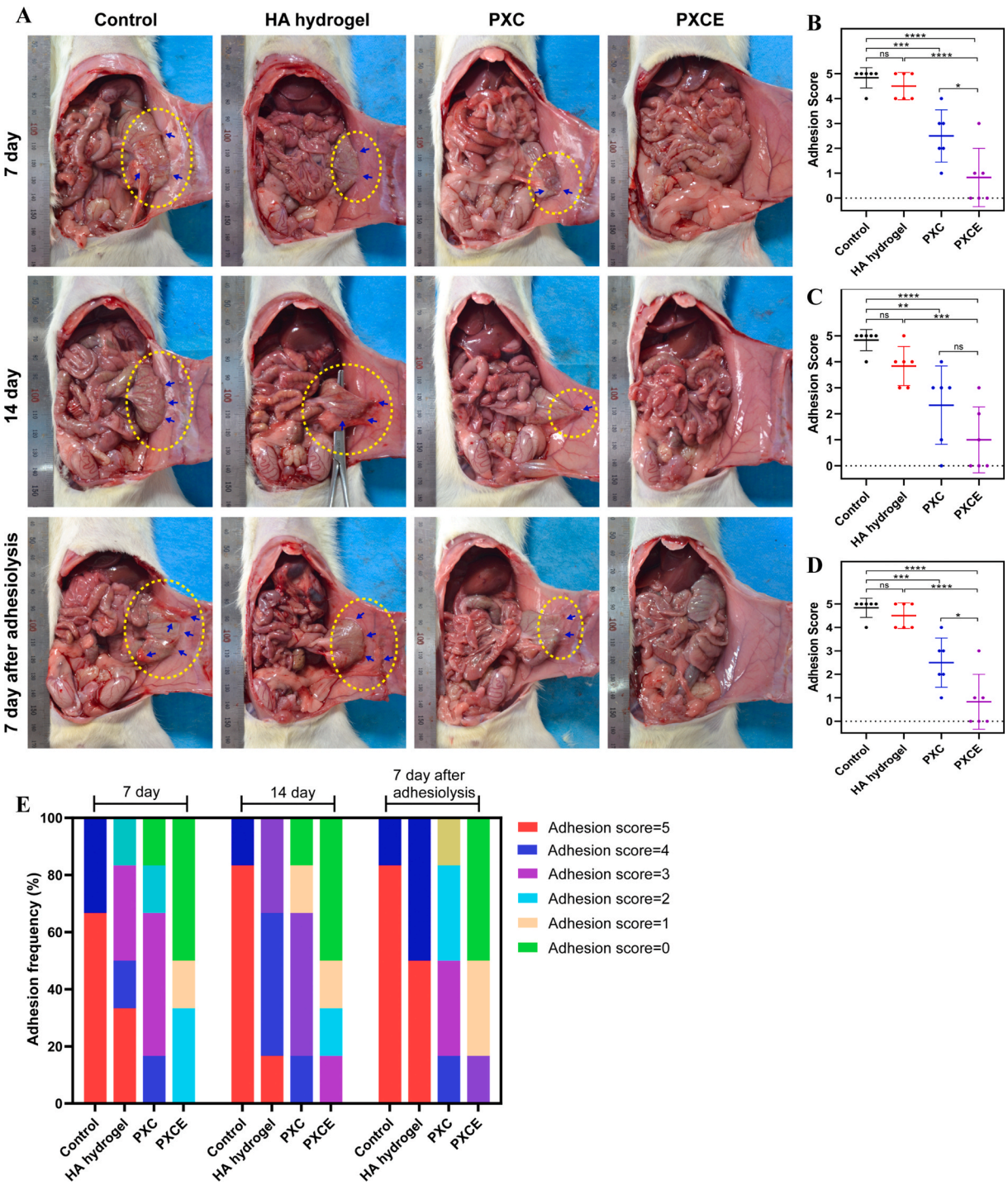

Fig. 4. Gross observations and adhesion scores. A) Representative images of abdominal adhesions in the control, HA, PXC, and PXCE group on day 7, day 14 following the initial operation, and day 7 after adhesiolysis. The adhesion area is indicated by a yellow oval; B) Gross assessment of adhesion score on day 7, C) day 14 after the primary surgery, and D) day 7 after adhesiolysis (n = 6); E) Distribution of adhesion scores in each group. (For interpretation of the references to color in this figure legend, the reader is referred to the Web version of this article.)

adhesion scores across various groups. It became apparent that the majority of scores in the control group were 4 and 5, whereas the PXCE group predominantly scored 0 and 1. The HA group and the PXC group occupied an intermediate position between the control and PXCE groups in terms of their scores.

Adhesion tissue specimens were obtained from various groups, and the abdominal adhesion grade and histological healing of the injured area were assessed using H&E and Masson staining (Fig. 5A and B). On day seven after the primary operation (Fig. 5A), the control group exhibited extensive and thick adhesion tissues, and the continuity of the peritoneum was interrupted. In particular, the injured skeletal muscle of the abdominal wall and the injured cecal smooth muscle layer adhered together due to adhesion tissues, resulting in evident fibrous connective tissue hyperplasia and the formation of a dense adhesion zone. H&E staining indicated the presence of numerous granulation tissues and inflammatory cells within the adhesion tissue, while Masson staining revealed significant deposition of collagen fibrils (marked by intense blue areas). Consistently, thick and dense adhesion areas were observed

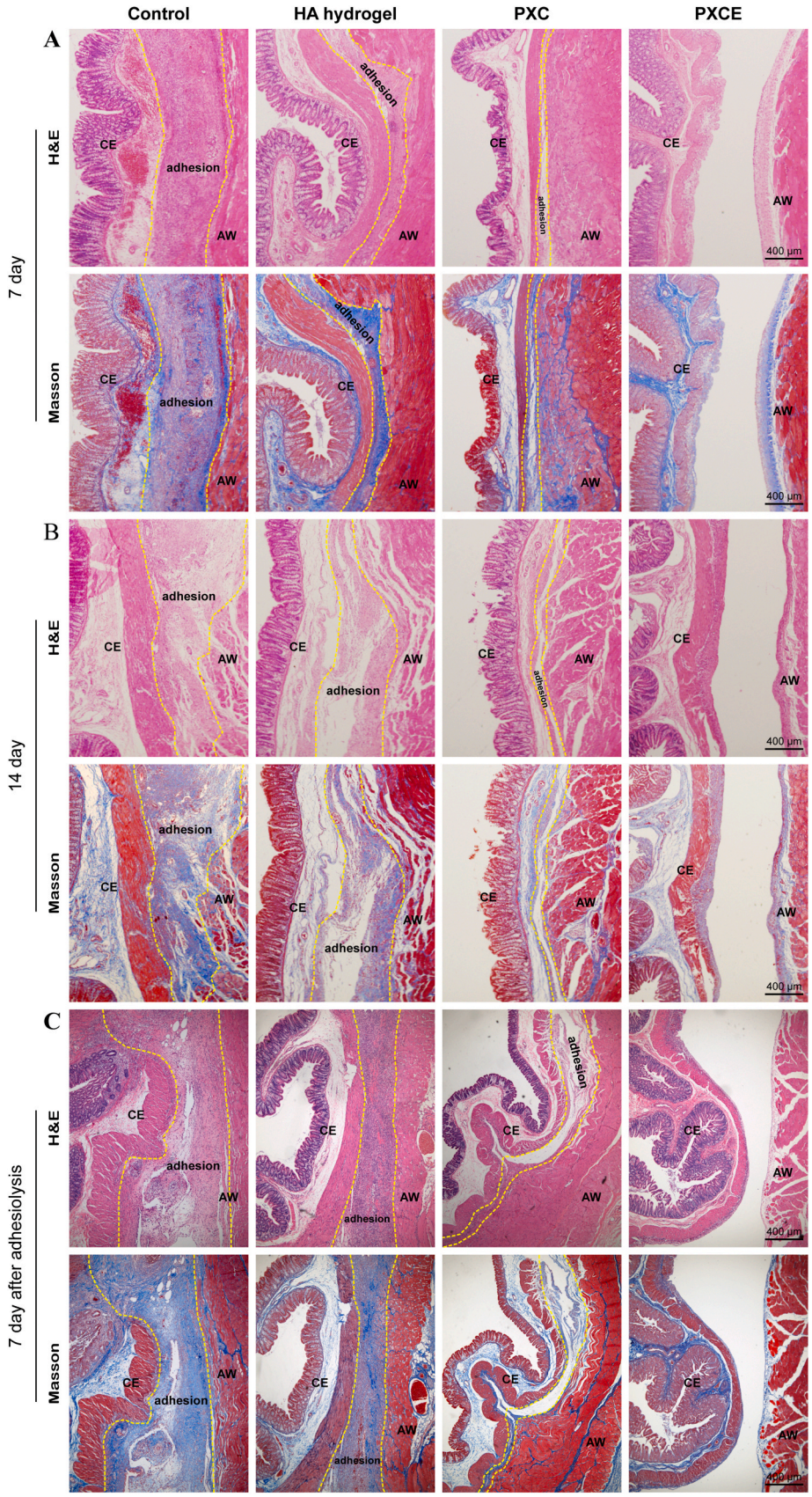

Fig. 5. Histological analysis (H&E staining and Masson's trichrome staining.) of adhesion specimens in the control group. A) HA, PXC, and PXCE group on day 7 after the first operation; B) HA, PXC, and PXCE group on day 14 following the initial operation; C) HA, PXC, and PXCE group on day 7 after adhesiolysis. CE for cecum, AW for abdominal wall; the adhesion region is delineated by a yellow dashed line. (For interpretation of the references to color in this figure legend, the reader is referred to the Web version of this article.)

on day 14 after the first operation (Fig. 5B). Furthermore, abundant neovascularizations were observed within the adhesion zone, suggesting the development of mature adhesions. On day 7, the HA group exhibited substantial adhesion as well. Although the adhesion area was slightly reduced and thinner compared to the untreated group, there remained noticeable infiltration of inflammatory cells and collagen deposition. On day 14, the adhesion region was seen, with evident connective tissue hyperplasia. For the PXC group, a thin layer of adhesion band was identified on day 7. The adhesion area exhibited reduced tightness, accompanied by a decrease in both inflammatory cell infiltration and collagen deposition. Similar results were also observed on day 14. In contrast to the aforementioned groups, the PXCE group did not exhibit any noticeable adhesion on either day 7 or day 14 following the initial surgery (Fig. 5A and B). Histologically, the surface of the injured area was covered with mesothelial cells. The peritoneal mesothelial cell layer was repaired neatly and continuously, and the inflammatory cell infiltration was minimal. In addition, Masson staining displayed little connective tissue and collagen deposition. Overall, these results strongly indicated that PXCE hydrogel had the potential to completely and reliably prevented PPA without affecting normal wound healing.

3.7. Evaluation of anti-adhesion efficacy on recurrent adhesions in repeated-injury adhesion model

Currently, adhesiolysis is the most effective clinical practice in managing severe complications caused by adhesions, such as intractable adhesive bowel obstruction and stubborn abdominal pain [57,58]. Occasionally, some patients need to undergo reoperation or multiple abdominal operations when a single treatment is not satisfied. The first step in the whole reoperation is to decompose the adhesions caused by primary surgery and clarify the anatomical structure before continuing the subsequent surgical procedures. The release of adhesions can temporarily relieve symptoms, but the incidence of recurrent adhesions remains high, regardless of surgical method (i.e., minimally invasive laparoscopy or general laparotomy). Similarly, recurrent adhesions can result in more severe complications. Preventing recurrent adhesions following adhesiolysis poses greater challenges in practice due to the severe trauma and the complex mechanism of secondary adhesion formation [59]. Despite the clinical use of various physical barrier materials (e.g., Interceed and commercial HA hydrogel), there is room for improvement in preventing the recurrence of adhesions, as these methods primarily target the prevention of primary adhesions. It is worth noting that certain studies have reported that certain materials exhibited significant efficacy in the classical cecum-abdominal wall abrasion model but failed to produce efficacy in the repeated-injury model, which was stricter and more biologically relevant. In this study, a more stringent rat adhesion model with repeated injuries was developed, and subsequently, the efficacy of PXC and PXCE hydrogels in preventing adhesions post-adhesiolysis was assessed (Fig. S7). The repeated-injury adhesion model was created by conducting adhesiolysis on day 7 following the initial modeling. On day 7 post-adhesiolysis, the control group displayed severe adhesion, characterized by a wide adhesion region and firm adhesion band necessitating sharp dissection. Without effective timely interventions after adhesiolysis, recurrent adhesion was almost inevitable and the adhesion degree is likely to be more serious than that formed after the initial operation. The HA hydrogel exerted an anti-adhesion effect on the formation of primary adhesion, but its efficacy on the repeated-injury model was poor. The PXC group demonstrated a respectable anti-adhesion effect in comparison to the control group. In contrast, the PXCE group exhibited the best anti-adhesion ability, not only effectively preventing primary adhesions but also inhibiting recurrent adhesions (Fig. 4A, B, C and D).

Histological analysis conducted on day 7 after surgery revealed a significant formation of vascularized adhesions in the control group, characterized by the presence of a dense adhesion region (Fig. 5C). Masson staining displayed substantial collagen deposition. Normally, secondary damage from adhesiolysis led to more severe adhesions. The hyperplasia of connective tissue and infiltration of inflammatory cells indicated that the HA hydrogel had limited effectiveness in preventing recurrent adhesions. In contrast, the PXC group showed the presence of adhesion formation, albeit with a thinner adhesion band, looser adhesion tissue, and a smaller adhesion area compared to the other groups. In addition, there was an alleviation of inflammation and fibrosis. Significantly, the PXCE group exhibited the most superior anti-adhesion efficacy: histological sections observed no obvious adhesion band, allowing for clear visualization of each layer's structure. The scraped wounds on the cecum and abdominal wall were nearly fully healed, with the mesothelial layer on the peritoneal surface returning to its original state. In brief, the exceptional anti-adhesion ability of the PXCE hydrogel can be attributed to a combination of its beneficial physiochemical properties, including good injectability, self-healing properties, and adhesion to the injured surface. Specifically, the hydrogel could be injected from a syringe, cover the injured surface, and function as a physical barrier by rapidly recovering from a fragmented state to a full gel state. Additionally, the PXCE hydrogel demonstrates the dual functionality of acting as a physical barrier while providing sustained release of ES.

3.8. Preliminary exploration of the mechanism of PXCE hydrogel in preventing adhesions

The local inflammatory response plays a crucial role in adhesion development. Following tissue injury, cells in the injured area release inflammatory mediators, promoting the aggregation of inflammatory cells. These cells subsequently release inflammatory cytokines like IL-6 and TNF-α, thereby intensifying the inflammatory reactions. TNF-α, a pivotal pro-inflammatory factor, can enhance downstream cytokines such as IL-6 and IL-8, leading to a local inflammatory imbalance in adhesions [60–62]. Moreover, TNF-α contributes to fibrinolysis imbalance by enhancing plasminogen activator expression and stimulating fibroblast proliferation. To obtain insights into the anti-adhesion pathways of as-prepared hydrogels, we collected serum samples from rats on day 7 after primary surgery for ELISA detection. The animal experiments revealed that the control group exhibited notably higher expression levels of inflammatory factors compared to the normal rats. In contrast, the HA group showed lower cytokine levels, although the reduction was not as pronounced as in the PXC and PXCE groups, respectively. As anticipated, both IL-6 and TNF-α levels decreased significantly in the PXC and PXCE groups. Particularly noteworthy was that the PXCE group displayed the least IL-6 and TNF-α levels, akin to those observed in normal rats. This finding strongly suggested that the PXCE hydrogel possesses a discernible anti-inflammatory effect (Fig. 6A and B).

Another crucial mechanism of adhesion formation is fibrosis, which primarily occurs due to the activation of myofibroblasts. TGF-β1, plays a significant role in promoting fibrosis [63–65]. Specifically, TGF-β1 activates myofibroblasts by regulating canonical (Smads-based) and non-canonical (non-Smads-dependent) signaling pathways, resulting in the accumulation of ECM components. Our experimental findings suggested that the levels of TGF-β1 decreased to different extents in the HA, PXC, and PXCE groups compared to the control group (Fig. 6C). Of these, the most significant decrease was observed in the PXCE group, approaching levels similar to those in normal rats. In addition, we stained the myofibroblasts marker α-SMA in the adhesion tissue through IHC (Fig. 6D). IHC data indicated that treatment with HA, PXC, and PXCE could reduce the number of α-SMA positive myofibroblasts to different extents, with PXCE performing the best (Fig. 6E). Previous studies have reported that ES has anti-fibrotic properties at its carboxyl-terminal part, which partly explains the good performance of PXCE hydrogels in inhibiting fibrosis [66,67]. In summary, our results demonstrated that PXCE hydrogel effectively inhibited the aberrant activation of local myofibroblasts and suppressed excessive collagen deposition.

Neovascularization plays a crucial role in providing nutrients to

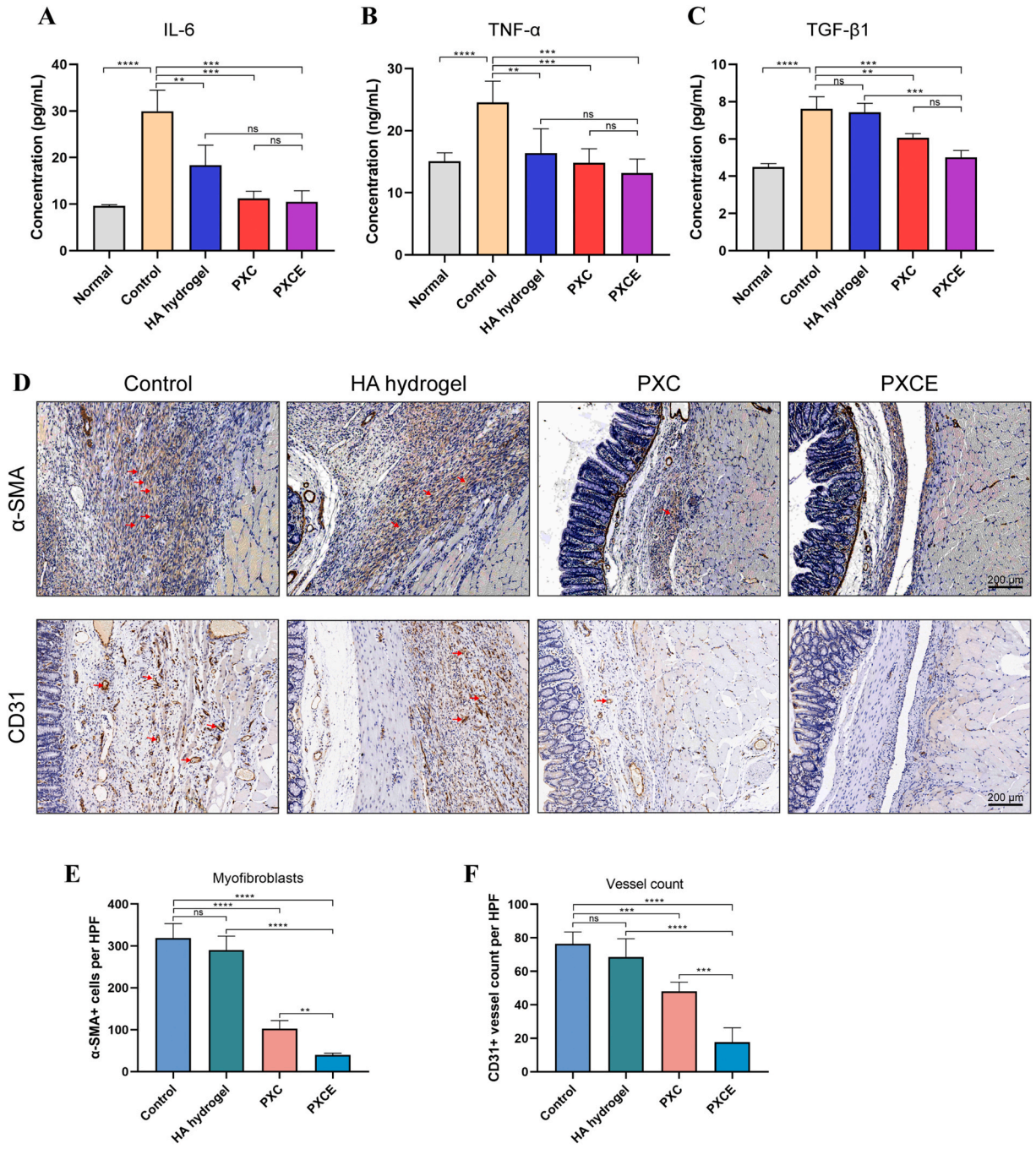

Fig. 6. Preliminary exploration of the potential mechanism of hydrogel for preventing post-operative adhesions. A) Serum levels for IL-6 were detected by ELISA; B) Serum levels for TNF- α were detected by ELISA; C) Serum levels for TGF-β1 were detected by ELISA; D) Representative images of immunostaining for α-SMA (myofibroblast marker), and CD31 (vascular endothelial cell marker) in the section of adhesion tissues; E) Histomorphometric quantification of α-SMA; F) Histomorphometric quantification of CD31. MF, microscopic field (10x); SMA, smooth muscle actin.

fibroblasts in the adhesion region and is a significant factor in adhesion formation. Previous studies have established the close association between vascularization of adhesion tissue and the development of mature adhesion [68,69]. Accordingly, we analyzed the effect of PXCE hydrogel on vascularization using the IHC method. To observe the neovascularization in adhesion bands, we stained CD31, a vascular endothelial cell marker, and a commonly-used indicator to evaluate angiogenesis [70] (Fig. 6D). Quantitative analysis of CD31-labeled sections demonstrated that the control group exhibited the highest count of new vessels, followed by the HA group, and the PXC group (Fig. 6F). Noteworthy, the PXCE group demonstrated a notable anti-angiogenesis effect, showing only a sparse presence of new vessels in high-magnification fields, the level significantly lower than that observed in other groups (all $p < 0.05$). This outcome aligns with our expectations: ES is a clinically-applied polypeptide drug with an anti-angiogenesis function. A high-dose application can cause some side effects, while a low-dose controlled release in the local region can avoid its adverse reactions. By employing a controlled-release strategy, PXCE achieves an outstanding anti-adhesion effect, addressing the challenge of adhesion formation while avoiding potential adverse reactions associated with high-dose ES administration.

3.9. In vivo retention time and biocompatibility of PXCE hydrogel

Numerous previous studies have demonstrated the ability of FITC-labeled hydrogel as an accurate tracking method [71]. We utilized FITC as the hydrogel tracer, the in vivo retention times of PXC hydrogel and PXCE hydrogel are shown in Fig. 7, respectively. Following surgical procedures in the animal models, FITC-labeled hydrogel samples were administered to cover the injured regions. On day 0 (2 h after the operation), the abdominal cavity was observed with strong fluorescent signals, which remained concentrated in the scraping area, indicating good tissue-adhesion ability to biological tissues. Over time, the area of orange-red fluorescence gradually decreased, suggesting that the hydrogel was gradually degraded. On day 7, only a small part of the hydrogel remained while on day 10, the fluorescence almost completely disappeared, suggesting that the hydrogel samples were degraded. In contrast, there was no fluorescence signal in the abdominal cavity on day 14. Interestingly, the degradation curves of PXC and PXCE hydrogels showed consistency, indicating that the incorporation of ES into PXC hydrogel had minimal impact on its overall stability. It is well-established in the field that the critical period for adhesion formation is within the first seven days after surgery. Therefore, it is crucial to implement effective interventions within this period to prevent adhesion. Remarkably, the in vivo retention time of the PXC and PXCE hydrogels is about 10 days, aligning with the optimal degradation duration necessary to cover the crucial seven-day period. Collectively, the PXCE hydrogel exerted dual effects as a physical barrier and drug release within the seven-day crucial period. Additionally, beyond this time frame, the hydrogel can be completely absorbed without eliciting any foreign body rejection response.

To meet the criteria of an ideal anti-adhesion biomaterial, it is crucial for the material to possess good biocompatibility, meaning it can be continuously degraded and absorbed into the blood without causing any damage to blood cells and major organs. The hemolysis assay conducted revealed that both the PXC and PXCE hydrogels demonstrated hemolysis ratios of lower than 2 % (Fig. S8), indicating their excellent hemocompatibility. Tissue sections of major organs were collected on days 7 and 14 exhibited no necrosis or inflammatory reactions upon PXC and PXCE hydrogel treatments when compared with healthy tissues (Fig. S9), confirming their low organ toxicity and high biocompatibility. Adhesion ability also is of vital importance for hydrogel adhering to wound tissue. As shown in Fig. S10, two fresh abdominal tissue pieces from rats were bonded with PXC hydrogel and PXCE hydrogel, respectively, which intuitively suggested that both PXC hydrogel and PXCE hydrogel all had biological tissue adhesion ability.

4. Conclusion

In this contribution, we have successfully integrated physical barrier and pharmacotherapy strategies to develop a highly versatile drug-loaded hydrogel. The drug-loaded hydrogel PXCE, loaded with the drug ES, demonstrated several outstanding characteristics, including prolonged the retention time of ES in vivo, increased local concentration of ES, excellent biocompatibility, injectability, self-healing properties, degradability, and stable and sustained ES controlled release in a stable and sustained manner. Importantly, as-prepared hydrogel exhibited remarkable efficacy in preventing primary and recurrent PPA in animal experiments. The injectable nature of this kind of hydrogels, combined with their tissue-adhesive, and self-fused peptide-loaded properties,

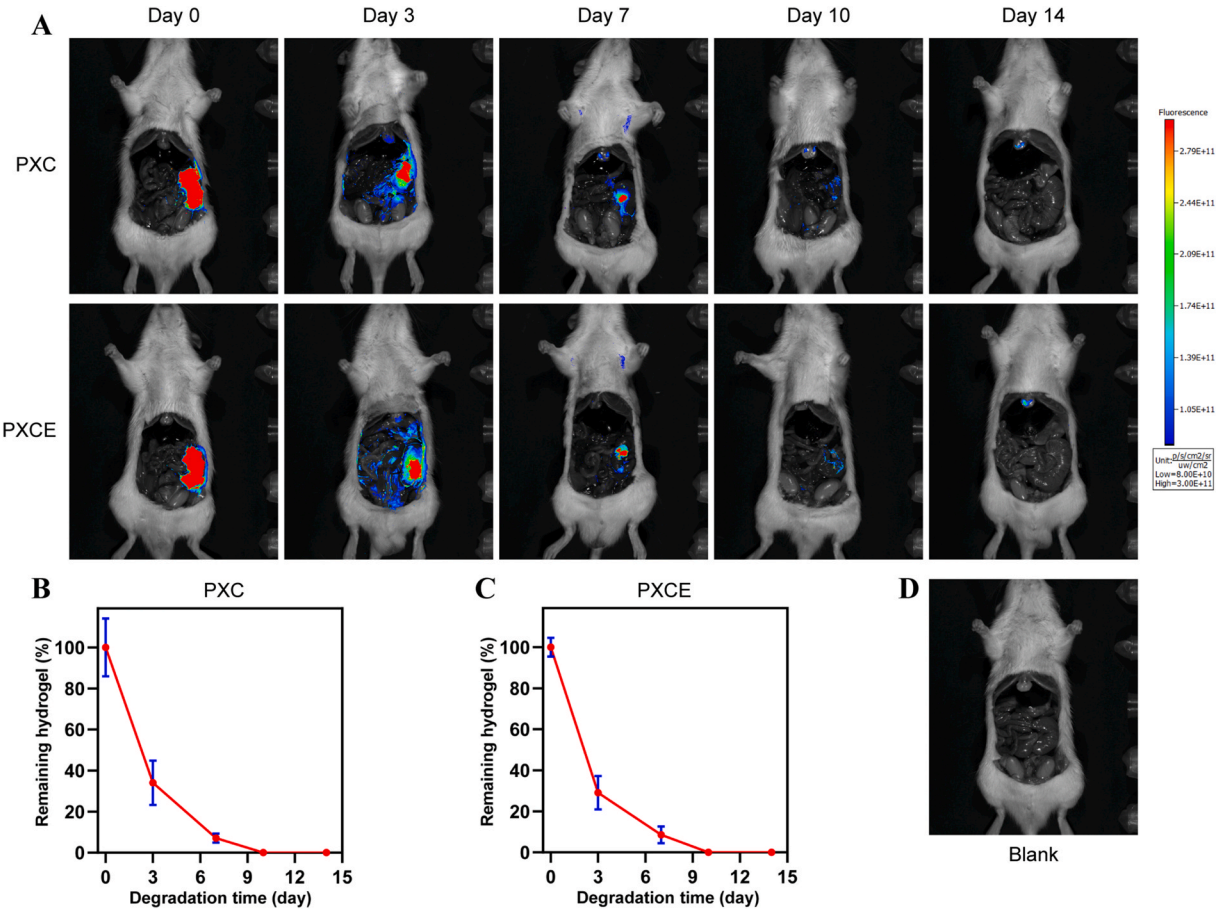

Fig. 7. In vivo retention time of PXC and PXCE hydrogels. A) Living imaging of the FITC-labeled PXC and PXCE hydrogels in the abdominal cavity; B) Degradation curve of PXC; C) Degradation curve of PXCE hydrogels in vivo; D) Blank.

opens up new possibilities for local controlled release of small molecule peptide drugs. Offering an innovative approach to the controlled release of peptide drugs at the application site, our injectable hydrogel has the potential to transform the field and facilitate the creation of anti-adhesion materials that are both more effective and efficient.

CRediT authorship contribution statement

Zequn Zhang: Writing – original draft, Investigation, Formal analysis, Data curation. **Chao Yin:** Writing – original draft, Investigation, Formal analysis, Data curation. **Xianwen Song:** Writing – review & editing, Data curation. **Xi Liu:** Writing – review & editing, Data curation. **Chonglei Zhong:** Writing – review & editing, Supervision. **Jun Zheng:** Resources, Data curation. **Yaqiong Ni:** Validation, Data curation. **Rujuan Shen:** Resources. **Yihang Guo:** Resources, Funding acquisition. **Xiaorong Li:** Writing – review & editing, Supervision, Project administration. **Changwei Lin:** Supervision, Data curation. **Yi Zhang:** Writing – review & editing, Supervision, Project administration, Funding acquisition. **Gui Hu:** Resources, Project administration, Funding acquisition.

Declaration of competing interest

The authors declare that they have no known competing financial interests or personal relationships that could have appeared to influence the work reported in this paper.

Data availability

Data will be made available on request.

Acknowledgments

The National Natural Science Foundation of China (No. 82172833, 21972169, 21773311), Hunan Provincial Science and Technology Plan Project (2022RC1218, 2019TP1001), Hunan Provincial Science and Technology Plan Project, China (2023JJ30824); Hunan Association for Science and Technology (2023TJ-N18) and Fundamental Research Funds for the Central Universities of Central South University (1053320230877), were acknowledged for the financial support. The authors would like to thank eceshi (www.eceshi.com) for XRD surveys.

Appendix A. Supplementary data

Supplementary data to this article can be found online at https://doi.org/10.1016/j.mtbio.2024.101205.

References

[1] D. Moris, J. Chakedis, A.A. Rahnemai-Azar, A. Wilson, M.M. Hennessy, A. Athanasiou, E.W. Beal, C. Argyrou, E. Felekouras, T.M. Pawlik, Postoperative abdominal adhesions: clinical significance and advances in prevention and management, J. Gastrointest. Surg. 21 (10) (2017) 1713–1722.
[2] T. Ito, Y. Shintani, L. Fields, M. Shiraishi, M.N. Podaru, S. Kainuma, K. Yamashita, K. Kobayashi, M. Perretti, F. Lewis-McDougall, K. Suzuki, Cell barrier function of resident peritoneal macrophages in post-operative adhesions, Nat. Commun. 12 (1) (2021) 2232.
[3] F.I. Scott, R.K. Vajravelu, R. Mamtani, N. Bianchina, N. Mahmoud, J.K. Hou, Q. Wu, X. Wang, K. Haynes, J.D. Lewis, Association between statin use at the time of intra-abdominal surgery and postoperative adhesion-related complications and small-bowel obstruction, JAMA Netw. Open 4 (2) (2021) e2036315.
[4] G.U. Ruiz-Esparza, X. Wang, X. Zhang, S. Jimenez-Vazquez, L. Diaz-Gomez, A. M. Lavoie, S. Afewerki, A.A. Fuentes-Baldemar, R. Parra-Saldivar, N. Jiang, N. Annabi, B. Saleh, A.K. Yetisen, A. Sheikhi, T.H. Jozefiak, S.R. Shin, N. Dong, A. Khademhosseini, Nanoengineered shear-thinning hydrogel barrier for preventing postoperative abdominal adhesions, Nano-Micro Lett. 13 (1) (2021) 1–16.
[5] H. Atta, M. El-Rehany, E. Roeb, H. Abdel-Ghany, M. Ramzy, S. Gaber, Mutant matrix metalloproteinase-9 reduces postoperative peritoneal adhesions in rats, Int. J. Surg. 26 (2016) 58–63.
[6] M.W.J. Stommel, R.P.G. ten Broek, C. Strik, G.D. Slooter, C. Verhoef, D. J. Grunhagen, P. van Dutjvendijk, M.H.A. Bemelmans, M. den Dulk, C. Sietses, T.N. T. van Heek, P.B. van den Boezem, J.H.W. de Wilt, H. van Goor, Multicenter observational study of adhesion formation after open-and laparoscopic surgery for colorectal cancer, Ann. Surg. 267 (4) (2018) 743–748.
[7] T. Kucukozkan, B. Ersoy, D. Uygur, C. Gundogdu, Prevention of adhesions by sodium chromoglycate, dexamethasone, saline and aprotinin after pelvic surgery, ANZ J. Surg. 74 (12) (2004) 1111–1115.
[8] J. Tang, Z. Xiang, M.T. Bernards, S. Chen, Peritoneal adhesions: occurrence, prevention and experimental models, Acta Biomater. 116 (2020) 84–104.
[9] J. Li, W. Xu, J. Chen, D. Li, K. Zhang, T. Liu, J. Ding, X. Chen, Highly bioadhesive polymer membrane continuously releases cytostatic and anti-inflammatory drugs for peritoneal adhesion prevention, ACS Biomater. Sci. Eng. 4 (6) (2018) 2026–2036.
[10] R.P.G. ten Broek, M.W.J. Stommel, C. Strik, C.J.H.M. van Laarhoven, F. Keus, H. van Goor, Benefits and harms of adhesion barriers for abdominal surgery: a systematic review and meta-analysis, Lancet 383 (9911) (2014) 48–59.
[11] A.K.S. Chandel, A. Shimizu, K. Hasegawa, T. Ito, Advancement of biomaterial-based postoperative adhesion barriers, Macromol. Biosci. 21 (3) (2021) 2000395.
[12] T.K. Rajab, M. Wallwiener, C. Planck, C. Brochhausen, B. Kraemer, C. W. Wallwiener, A direct comparison of Seprafilm, adept, intercoat, and spraygel for adhesion prophylaxis, J. Surg. Res. 161 (2) (2010) 246–249.
[13] X. Wu, W. Guo, L. Wang, Y. Xu, Z. Wang, Y. Yang, L. Yu, J. Huang, Y. Li, H. Zhang, Y. Wu, G. Li, W. Huang, An injectable asymmetric-adhesive hydrogel as a GATA6^{+} cavity macrophage trap to prevent the formation of postoperative adhesions after minimally invasive surgery, Adv. Funct. Mater. 32 (9) (2022) 2110066.
[14] W. Arung, M. Meurisse, O. Detry, Pathophysiology and prevention of postoperative peritoneal adhesions, World J. Gastroenterol. 17 (41) (2011) 4545–4553.
[15] B.W.J. Hellebrekers, T. Kooistra, Pathogenesis of postoperative adhesion formation, Br. J. Surg. 98 (11) (2011) 1503–1516.
[16] D.S. Foster, C.D. Marshall, G.S. Gulati, M.S. Chinta, A. Nguyen, A. Salhotra, R. E. Jones, A. Burcham, T. Lerbs, L. Cui, M.E. King, A.L. Titan, R.C. Ransom, A. Manjunath, M.S. Hu, C.P. Blackshear, S. Mascharak, A.L. Moore, J.A. Norton, C. J. Kin, A.A. Shelton, M. Januszyk, G.C. Gurtner, G. Wernig, M.T. Longaker, Elucidating the fundamental fibrotic processes driving abdominal adhesion formation, Nat. Commun. 11 (1) (2020) 4061.
[17] Q. Hu, X. Xia, X. Kang, P. Song, Z. Liu, M. Wang, W. Guan, S. Liu, A review of physiological and cellular mechanisms underlying fibrotic postoperative adhesion, Int. J. Biol. Sci. 17 (1) (2021) 298–306.
[18] B.Z. Johnson, A.W. Stevenson, C.M. Prêle, M.W. Fear, F.M. Wood, The role of IL-6 in skin fibrosis and cutaneous wound healing, Biomedicines 8 (5) (2020) 101.
[19] S.E. Herrick, B. Wilm, Post-surgical peritoneal scarring and key molecular mechanisms, Biomolecules 11 (5) (2021) 692.
[20] B. Liu, Y. Kong, O.A. Alimi, M.A. Kuss, H. Tu, W. Hu, A. Rafay, K. Vikas, W. Shi, M. Lerner, W.L. Berry, Y. Li, M.A. Carlson, B. Duan, Multifunctional microgel-based cream hydrogels for postoperative abdominal adhesion prevention, ACS Nano 17 (4) (2023) 3847–3864.
[21] X. Liu, X. Song, Z. Zhang, S. Yang, L. Li, C. Lin, M. Chen, C. Liu, X. Li, Y. Zhang, G. Hu, Multifunctional oxidized dextran–metformin as a tissue-adhesive hydrogel to prevent postoperative peritoneal adhesions in patients with metabolic syndrome, Adv. Sci. 10 (33) (2023) 2303767.
[22] X. Song, Z. Zhang, Z. Shen, J. Zheng, X. Liu, Y. Ni, J. Quan, X. Li, G. Hu, Y. Zhang, Facile preparation of drug-releasing supramolecular hydrogel for preventing postoperative peritoneal adhesion, ACS Appl. Mater. Interfaces 13 (48) (2021) 56881–56891.
[23] Y. Gou, Y. Weng, Q. Chen, J. Wu, H. Wang, J. Zhong, Y. Bi, D. Cao, P. Zhao, X. Dong, M. Guo, W. Wagstaff, B. Hendren-Santiago, C. Chen, A. Youssef, R. C. Haydon, H.H. Luu, R.R. Reid, L. Shen, T.C. He, J. Fan, Carboxymethyl chitosan prolongs adenovirus-mediated expression of IL-10 and ameliorates hepatic fibrosis in a mouse model, Bioeng. transl. med. 7 (2022) e10306.
[24] Z. Xu, L. Zou, F. Xie, X. Zhang, X. Ou, G. Gao, Biocompatible carboxymethyl chitosan/GO-based sponge to improve the efficiency of hemostasis and wound healing, ACS appl. Mater. Inter. 14 (2022) 44799–44808.
[25] Z. Shariatinia, Carboxymethyl chitosan: properties and biomedical applications, Int. J. Biol. Macromol. 120 (2018) 1406–1419.
[26] L. Upadhyaya, J. Singh, V. Agarwal, R.P. Tewari, Biomedical applications of carboxymethyl chitosans, Carbohydr. Polym. 91 (2013) 452–466.
[27] M.S.H. Akash, K. Rehman, S.Q. Chen, Pluronic F127-based thermosensitive gels for delivery of therapeutic proteins and peptides, Polym. Rev. 54 (2014) 573–597.
[28] A. Hardiansyah, A. Randy, R.T. Dewi, M. Angelina, N. Yudasari, S. Rahayu, I. M. Ulfah, F. Maryani, Y.W. Cheng, T.Y. Liu, Magnetic graphene-based nanosheets with Pluronic F127-chitosan biopolymers encapsulated α-mangosteen drugs for breast cancer cells therapy, Polymers-Basel 14 (2022) 3163–3177.
[29] A. Shafiq, A. Madni, S. Khan, H. Sultana, Sumaira, H. Shah, S. Khan, S. Rehman, M. Nawaz, Core-shell Pluronic F127/chitosan based nanoparticles for effective delivery of methotrexate in the management of rheumatoid arthritis, Int. J. Biol. Macromol. 213 (2022) 465–477.
[30] Y. Zhou, X.L. Zhang, S.T. Lu, N.Y. Zhang, H.J. Zhang, J. Zhang, J. Zhang, Human adipose-derived mesenchymal stem cells-derived exosomes encapsulated in pluronic F127 hydrogel promote wound healing and regeneration, Stem Cell Res. Ther. 13 (2022) 1–17.
[31] B. Kaczmarek-Szczepańska, O. Mazur, M. Michalska-Sionkowska, K. Łukowicz, A. M. Osyczka, The preparation and characterization of chitosan-based hydrogels cross-linked by glyoxal, Materials 14 (9) (2021) 2449.
[32] L. Wang, J.P. Stegemann, Glyoxal crosslinking of cell-seeded chitosan/collagen hydrogels for bone regeneration, Acta Biomater. 7 (6) (2011) 2410–2417.

[33] M. Zhang, C. Huang, J. Ou, F. Liu, S. Ou, J. Zheng, Glyoxal in foods: formation, metabolism, health hazards, and its control strategies, J. Agric. Food Chem. 72 (5) (2024) 2434–2450.
[34] C.C. Tsai, T.H. Young, G.S. Chen, N.C. Cheng, Developing a glyoxal-crosslinked chitosan/gelatin hydrogel for sustained release of human platelet lysate to promote tissue regeneration, Int. J. Mol. Sci. 22 (12) (2021) 6451.
[35] M. Dessì, A. Borzacchiello, T.H. Mohamed, W.I. Abdel-Fattah, L. Ambrosio, Novel biomimetic thermosensitive β-tricalcium phosphate/chitosan-based hydrogels for bone tissue engineering, J. Biomed. Mater. Res., Part A 101 (10) (2013) 2984–2993.
[36] A. Dasgupta, N. Sori, S. Petrova, Y. Maghdouri-White, N. Thayer, N. Kemper, S. Polk, D. Leathers, K. Coughenour, J. Dascoli, R. Palikonda, Comprehensive collagen crosslinking comparison of microfluidic wet-extruded microfibers for bioactive surgical suture development, Acta Biomater. 128 (2021) 186–200.
[37] H. Kosaka, T. Yoshimoto, T. Yoshimoto, J. Fujimoto, K. Nakanishi, Interferon-gamma is a therapeutic target molecule for prevention of postoperative adhesion formation, Nat. Med. 14 (4) (2008) 437–441.
[38] D.R. Chung, T. Chitnis, R.J. Panzo, D.L. Kasper, M.H. Sayegh, A.O. Tzianabos, CD4^{+} T cells regulate surgical and postinfectious adhesion formation, J. Exp. Med. 195 (11) (2002) 1471–1478.
[39] E. Zhang, B. Song, Y. Shi, H. Zhu, X. Han, H. Du, C. Yang, Z. Cao, Fouling-resistant zwitterionic polymers for complete prevention of postoperative adhesion, Proc. Natl. Acad. Sci. U.S.A. 117 (50) (2020) 32046–32055.
[40] J. Yu, K. Wang, C. Fan, X. Zhao, J. Gao, W. Jing, X. Zhang, J. Li, Y. Li, J. Yang, W. Liu, An ultrasoft self-fused supramolecular polymer hydrogel for completely preventing postoperative tissue adhesion, Adv. Mater. 33 (16) (2021) 2008395.
[41] L. Wang, Z. Luo, J. Yan, Z. Ban, M. Yang, M. Qi, Y. Xu, F. Wang, L. Li, Ultrasonic nebulization-assisted layer-by-layer assembly based on carboxymethyl chitosan: an emerging alternative for promoting phenylpropanoid metabolism, Ultrason. Sonochem. 68 (2020) 105184.
[42] F. Liu, D. Ma, X. Luo, Z. Zhang, L. He, Y. Gao, D.J. McClements, Fabrication and characterization of protein-phenolic conjugate nanoparticles for co-delivery of curcumin and resveratrol, Food Hydrocolloids 79 (2018) 450–461.
[43] X. Song, T. He, Y. Qi, Y. Liu, H. Wu, C. Liu, Y. Zhang, Properties of cell-compatible poly(vinyl alcohol) hydrogels cross-linked with hydrophobic luteolin, ACS Appl. Polym. Mater. 3 (6) (2021) 3019–3027.
[44] X. Wei, C. Cui, C. Fan, T. Wu, Y. Li, X. Zhang, K. Wang, Y. Pang, P. Yao, J. Yang, Injectable hydrogel based on dodecyl-modified N-carboxyethyl chitosan/oxidized konjac glucomannan effectively prevents bleeding and postoperative adhesions after partial hepatectomy, Int. J. Biol. Macromol. 199 (2022) 401–412.
[45] Q. Mao, O. Hoffmann, K. Yu, F. Lu, G. Lan, F. Dai, S. Shang, R. Xie, Self-contracting oxidized starch/gelatin hydrogel for noninvasive wound closure and wound healing, Mater. Des. 194 (2020) 108916.
[46] H. Helmick, C. Hartanto, A. Bhunia, A. Liceaga, J.L. Kokini, Validation of bioinformatic modeling for the zeta potential of vicilin, legumin, and commercial pea protein isolate, Food Biophys. 16 (2021) 474–483.
[47] M.E. Haghiri, A. Izanloo, Design and characterization of colloidal solution of manganese ferrite nanostructure coated with carboxymethyl chitosan, Mater. Chem. Phys. 216 (2018) 265–271.
[48] I. Pepić, J. Filipović-Grčić, I. Jalšenjak, Bulk properties of nonionic surfactant and chitosan mixtures, Colloids Surf. A Physicochem. Eng. Aspects 336 (1–3) (2009) 135–141.
[49] Z. Zhang, X. Liu, Z. Shen, J. Quan, C. Lin, X. Li, G. Hu, Endostatin in fibrosis and as a potential candidate of anti-fibrotic therapy, Drug Deliv. 28 (2021) 2051–2061.
[50] H. Ren, Y. Li, Y. Chen, L. Wang, Endostatin attenuates PDGF-BB- or TGF-beta1-induced HSCs activation via suppressing RhoA/ROCK1 signal pathways, Drug Des. Dev. Ther. 13 (2019) 285–290.
[51] M.S. O'reilly, T. Boehm, Y. Shing, N. Fukai, G. Vasios, W.S. Lane, E. Flynn, J. R. Birkhead, B.R. Olsen, J. Folkman, Endostatin: an endogenous inhibitor of angiogenesis and tumor growth, Cell 88 (1997) 277–285.
[52] Z. Wang, Y. Zhang, Y. Yin, J. Liu, P. Li, Y. Zhao, D. Bai, H. Zhao, X. Han, Q. Chen, High-strength and injectable supramolecular hydrogel self-assembled by monomeric nucleoside for tooth-extraction wound healing, Adv. Mater. 34 (13) (2022) 2108300.
[53] A. Fonseca-García, B.H. Osorio, R.Y. Aguirre-Loredo, H.L. Calambas, C. Caicedo, Miscibility study of thermoplastic starch/polylactic acid blends: thermal and superficial properties, Carbohydr. Polym. 293 (2022) 119744.
[54] X. Zhao, Y. Liang, Y. Huang, J. He, Y. Han, B. Guo, Physical double-network hydrogel adhesives with rapid shape adaptability, fast self-healing, antioxidant and NIR/pH stimulus-responsiveness for multidrug-resistant bacterial infection and removable wound dressing, Adv. Funct. Mater. 30 (17) (2020) 1910748.
[55] Y.F. Gong, X.M. Zhang, F. Liu, Z.Z. Wang, X.F. Deng, Y. Jiao, X.J. Li, X.Y. Huang, Inhibitory effect of recombinant human endostatin on the proliferation of hypertrophic scar fibroblasts in a rabbit ear model, Eur. J. Pharmacol. 791 (2016) 647–654.
[56] Y.F. Gong, X.M. Zhang, J. Yu, T.Y. Huang, Z.Z. Wang, F. Liu, X.Y. Huang, Effect of recombinant human endostatin on hypertrophic scar fibroblast apoptosis in a rabbit ear model, Biomed. Pharmacother. 91 (2017) 680–686.
[57] D.J. Swank, S.C.G. Swank-Bordewijk, W.C.J. Hop, Laparoscopic adhesiolysis in patients with chronic abdominal pain: a blinded randomised controlled multi-centre trial, Lancet 361 (9376) (2003) 2250.
[58] M.J. Molegraaf, B. Torensma, C.P. Lange, J.F. Lange, J. Jeekel, D.J. Swank, Twelve-year outcomes of laparoscopic adhesiolysis in patients with chronic abdominal pain: a randomized clinical trial, Surgery 161 (2) (2017) 415–421.
[59] P.R. Koninckx, V. Gomel, A. Ussia, L. Adamyan, Role of the peritoneal cavity in the prevention of postoperative adhesions, pain, and fatigue, Fertil. Steril. 106 (5) (2016) 998–1010.
[60] Y.C. Cheong, J.B. Shelton, S.M. Laird, M. Richmond, G. Kudesia, T.C. Li, W. L. Ledger, IL-1, IL-6 and TNF-alpha concentrations in the peritoneal fluid of women with pelvic adhesions, Hum. Reprod. 17 (1) (2002) 69–75.
[61] N. Uyama, H. Tsutsui, S. Wu, K. Yasuda, E. Hatano, X.Y. Qin, S. Kojima, J. Fujimoto, Anti-interleukin-6 receptor antibody treatment ameliorates postoperative adhesion formation, Sci. Rep. 9 (2019) 17558.
[62] X. Jin, S. Ren, E. Macarak, J. Rosenbloom, Pathobiological mechanisms of peritoneal adhesions: the mesenchymal transition of rat peritoneal mesothelial cells induced by TGF-beta 1 and IL-6 requires activation of Erk1/2 and Smad2 linker region phosphorylation, Matrix Biol. 51 (2016) 55–64.
[63] N. Chegini, TGF-beta system: the principal profibrotic mediator of peritoneal adhesion formation, Semin. Reprod. Med. 26 (4) (2008) 298–312.
[64] X.M. Meng, D.J. Nikolic-Paterson, H.Y. Lan, TGF-beta: the master regulator of fibrosis, Nat. Rev. Nephrol. 12 (6) (2016) 325–338.
[65] Z.D. Lv, D. Na, X.Y. Ma, C. Zhao, W.J. Zhao, H.M. Xu, Human peritoneal mesothelial cell transformation into myofibroblasts; in response to TGF-beta 1 in vitro, Int. J. Mol. Med. 27 (2) (2011) 187–193.
[66] Y. Yamaguchi, T. Takihara, R.A. Chambers, K.L. Veraldi, A.T. Larregina, C. A. Feghali-Bostwick, A peptide derived from endostatin ameliorates organ fibrosis, Sci. Transl. Med. 4 (136) (2012) 136ra71.
[67] T. Nishimoto, L. Mlakar, T. Takihara, C. Feghali-Bostwick, An endostatin-derived peptide orally exerts anti-fibrotic activity in a murine pulmonary fibrosis model, Int. Immunopharm. 28 (2) (2015) 1102–1105.
[68] M. Basbug, N. Bulbuller, C. Camci, R. Ayten, E. Aygen, I.H. Ozercan, Z. Arikanoglu, S. Akbulut, The effect of antivascular endothelial growth factor on the development of adhesion formation in laparotomized rats: experimental study, Gastroenterol. Res. Pract. 2011 (2011) 578691.
[69] G. Acun, H. Ozdemir, O. Sunamak, Z.U. Ozdemir, E. Baskan, M. Yazi, B. Savas, U. Berberoglu, The effect of single-dose intraperitoneal bevacizumab on peritoneal adhesion formation, Rev. Invest. Clin. 70 (6) (2018) 279–284.
[70] M.L. Biller, C. Tuffs, M. Bleul, D.T.-A. Tran, M. Dupovac, U. Keppler, J.M. Harnoss, P. Probst, M. Schneider, M.J. Strowitzki, Effect of metformin on HIF-1α signaling and postoperative adhesion formation, J. Am. Coll. Surg. 234 (6) (2022) 1167–1180.
[71] X. Zhao, J. Yang, Y. Liu, J. Gao, K. Wang, W. Liu, An injectable and antifouling self-fused supramolecular hydrogel for preventing postoperative and recurrent adhesions, Chem. Eng. J. 404 (2021) 127096.